Complete characterization of GaAs gradient-elastic tensors and reconstruction of internal strain in GaAs/AlGaAs quantum dots using nuclear magnetic resonance

I. M. Griffiths,[1] H. Huang,[2] A. Rastelli,[2] M. S. Skolnick,[1] and E. A. Chekhovich[1,*]
[1]*Department of Physics and Astronomy, University of Sheffield, Sheffield S3 7RH, United Kingdom*
[2]*Institute of Semiconductor and Solid State Physics, Johannes Kepler University Linz, Altenbergerstr. 69, 4040 Linz, Austria*

(Received 4 February 2019; published 20 March 2019)

Recently, we have calibrated the diagonal components $S_{11} = S_{xxxx}$ of the GaAs gradient elastic tensor S_{ijkl} using nuclear magnetic resonance (NMR) and photoluminescence spectroscopy of GaAs/AlGaAs quantum dot structures in Faraday geometry [E. A. Chekhovich *et al.*, Phys. Rev. B **97**, 235311 (2018)]. Here we measure quantum dot NMR spectra in oblique magnetic fields giving access to the off-diagonal components S_{yzyz}. We find the ratios $S_{yzyz}/S_{xxxx} \approx +1.98^{+0.21}_{-0.27}$ for ^{75}As and $\approx -0.40^{+0.23}_{-0.31}$ for ^{69}Ga. Combined with our previous results, we find all independent nonzero components of S_{ijkl}: $QS_{xxxx} \approx +0.758 \times 10^{-6}$ V, $QS_{yzyz} \approx +1.51 \times 10^{-6}$ V for ^{75}As and $QS_{xxxx} \approx -0.377 \times 10^{-6}$ V, $QS_{yzyz} \approx +0.151 \times 10^{-6}$ V for ^{69}Ga, where Q is the corresponding nuclear quadrupolar moment. Our results show that earlier nuclear acoustic resonance experiments [R. K. Sundfors, Phys. Rev. B **10**, 4244 (1974)] most likely overestimated the GaAs gradient elastic tensors, especially for ^{69}Ga. We further use NMR spectroscopy in oblique fields for assumption-free measurement of the intrinsic strain in GaAs/AlGaAs quantum dots. We find deviations of the strain principle directions from the sample growth axis, which vary between individual quantum dots.

DOI: 10.1103/PhysRevB.99.125304

I. INTRODUCTION

Elastic deformation of a solid body is described by a symmetric strain tensor ϵ_{ij}. In semiconductors, strain leads to a variety of effects arising from modification of electronic orbitals. One such effect is generation of electric field gradients (EFGs) at the atomic sites. EFGs are described by a tensor V_{kl}, and the traceless part of V_{kl} is readily observed in the nuclear magnetic resonance (NMR) spectra of quadrupolar nuclei (with spin $I > 1/2$). The relation between strain and the resulting EFGs is given by a fourth rank "gradient-elastic" tensor S_{ijkl}, via $V_{ij} = \sum_{k,l} S_{ijkl}\epsilon_{kl}$.

In solids with high crystal symmetry the number of nonzero independent components of S_{ijkl} is significantly reduced: in the case of cubic symmetry one usually uses [1] $S_{xxyy} = -S_{xxxx}/2$ and the gradient-elastic tensor is then fully described by the diagonal component S_{xxxx} ($=S_{yyyy} = S_{zzzz}$) and the off-diagonal component S_{yzyz} ($=S_{xyxy} = S_{xzxz}$). In order to disentangle the two tensor components at least two experiments conducted in different geometries are required [2]. In the nuclear acoustic resonance (NAR) experiments by Sundfors [3–5], acoustic waves with two different polarizations were used to derive $S_{11} = S_{xxxx}$ and $S_{44} = S_{yzyz}$ in GaAs and other III-V semiconductors (here S_{11} and S_{44} are the tensor components in Voigt notation). Bogdanov and Lemanov have conducted NMR experiments on III-V semiconductors under static stress and variable magnetic field orientations [6,7] but in the case of GaAs could not obtain S_{ijkl} reliably due to sample imperfections [7]. Recently we have conducted NMR experiments in a special configuration (Faraday geometry), where magnetic field is parallel to the [001] crystallographic axis, and uniaxial static stress is orthogonal to [001]. This experiment reveals the S_{xxxx} components on their own [8]. Our S_{xxxx} values for GaAs were found to be a factor of $\sim$1.4 smaller than in the early experiments by Sundfors [4], which highlight the need for reexamination of the S_{yzyz} values as well. Here we measure the S_{yzyz}/S_{xxxx} ratios in GaAs. Importantly, we conduct experiments in three different geometries giving an overcomplete set of measurements, and allowing the consistency of our results to be verified. Our S_{yzyz} values deviate significantly from the earlier NAR studies, especially for ^{69}Ga nuclei. Combining the results of this work with our previous report [8] we are able to provide a revised expression for the complete gradient-elastic tensors of gallium arsenide.

Accurate knowledge of S_{ijkl} is important for understanding and predicting the effect of strain on spin lifetimes [9] and spin coherence [10–15] in various GaAs based qubit systems. The S_{ijkl} tensors are also required for the nondestructive structural analysis approaches based on decoding the NMR spectra [16–26]. Here we present an example of such analysis. From first principles, we derive a closed-form relation between the strain ϵ_{ij} and the resulting NMR quadrupolar shift under arbitrary orientation of the static magnetic field. Using this model we are able to measure strain tensors in individual GaAs/AlGaAs quantum dots, without making any preliminary assumptions about the internal structure of the dots. We find for example that the symmetry (growth) axis of the planar GaAs/AlGaAs structure is not necessarily a symmetry axis of the quantum dot strain field: the deviation varies from dot to dot and can be on the order of $\approx 10^{\circ}$. This effect qualitatively correlates with the slightly irregular morphology of this type of GaAs/AlGaAs QDs as observed previously in

*e.chekhovich@sheffield.ac.uk

atomic force microscopy [27]. NMR strain profiling can be a valuable diagnostic tool in developing emerging quantum dot based devices, such as entangled photon sources, where fine-tuning, e.g., via strain fields, is crucial for achieving optimal performance. In this framework, only the presence of in-plane asymmetries have been considered up to now [28] and state-of-the-art results were obtained on selected QDs with regular morphology [29]. By contrast, it is still an open question whether an arbitrary QD (with a natural quantization axis tilted away from the growth axis) can reach the same performance.

II. EXPERIMENTAL TECHNIQUES AND SAMPLES

We study quantum dot structures grown using molecular beam epitaxy as described in our previous work [8]. Growth of aluminium droplets on AlGaAs is used to etch nanoholes [30,31] with a typical diameter of ∼40 nm and a depth of ∼5 nm, which are then filled with GaAs and capped with AlGaAs to form GaAs/AlGaAs quantum dots. We study an as-grown (unstressed) piece and a piece of the same sample stressed compressively along the [110] crystal axis using titanium bracket and screw [8]. The geometry of the experiment is shown in Fig. 1. A static magnetic field B_0 up to 10 T is applied. The excitation laser is parallel to the static field and is focused into a ∼1 μm spot on the sample surface by an aspheric lens. The photoluminescence (PL) signal is collimated by the same lens and analyzed with a grating spectrometer and a charge coupled device (CCD) camera. The orientation of the static magnetic field with respect to the sample crystallographic axes is described by angles θ and ϕ, which are varied by mounting the sample at different orientations. All experiments are conducted in a helium bath cryostat at a sample temperature ∼4.2 K. A small copper coil is mounted close to the sample and is used to generate radio frequency (rf) magnetic field B_{rf}. NMR spectra of individual quantum dots are measured using optical techniques developed [16] and described [8] previously. Key to these techniques are generation of large nuclear spin polarization via circularly polarized optical excitation [32] and optical measurement of the nuclear spin magnetization from the hyperfine shifts in QD PL spectra [33,34]. Unlike in bulk or thick quantum well structures [24], the strong spatial confinement of quantum dots ensures nearly pure heavy-hole ground exciton states, which facilitates large nuclear spin polarization leading to improved NMR sensitivity.

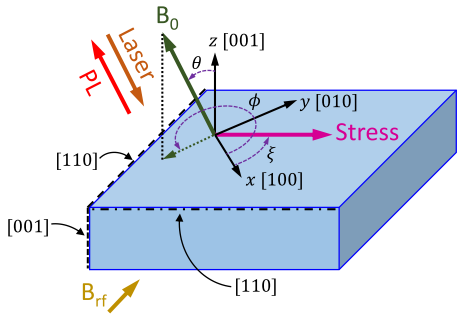

FIG. 1. Schematic of the experiment geometry. Coordinate system axes are aligned with the cubic crystal axes of the sample $x \parallel [100]$, $y \parallel [010]$, $z \parallel [001]$. The sample is grown along the [001] direction and cleaved along the [110] and [1$\bar{1}$0] directions. The direction of the static magnetic field B_0 is described by the polar angle θ between B_0 and z, and the azimuth angle ϕ which the projection of B_0 onto the xy plane makes with the x axis. External stress can be applied along the [110] direction, corresponding to azimuth angle $\xi = +45°$. The radio frequency field B_{rf} is orthogonal to both the B_0 and the stress directions.

III. THEORETICAL MODEL

The Hamiltonian of a nuclear spin I is a sum of the Zeeman term describing interaction of the nuclear magnetic dipole with the static magnetic field B_0 and a term describing interaction of the nuclear electric quadrupolar moment Q with EFGs [35–38]:

$$\hat{H} = -\frac{\gamma B_0}{2\pi}\hat{I}_z + \frac{eQ}{6I(2I-1)h}\sum_{i,j=x,y,z} V_{ij}\left(\frac{3}{2}(\hat{I}_i\hat{I}_j + \hat{I}_j\hat{I}_i) - \delta_{ij}I^2\right), \quad (1)$$

where the Hamiltonian is given in frequency units (Hz), e is the elementary charge, h is the Planck constant, and EFGs are described by a tensor $V_{\alpha\beta} = \frac{\partial^2 V}{\partial\alpha\partial\beta}$ $(\alpha, \beta = x, y, z)$ of the derivatives of the electrostatic potential $V(x, y, z)$. For $I = 3/2$ nuclei the time-independent Schrödinger equation is an eigenvalue problem with a 4×4 Hermitian matrix. A concise analytical solution can be found if the quadrupolar Hamiltonian is treated as a small perturbation to the Zeeman term. In this case, the effect of the quadrupolar interaction is that instead of a single NMR transition at the Larmor frequency $\nu_0 = \gamma B_0/(2\pi)$, a triplet of lines with spectral splitting ν_Q is observed [36–38]. The use of a first order approximation is justified since quadrupolar shifts in our experiments ($|\nu_Q| \leqslant$ 140 kHz) are at least a factor of 400 smaller than the Zeeman effect ($\nu_0 \geqslant 58$ MHz). The derivation is somewhat bulky and was performed with the aid of Wolfram Mathematica software (details can be found in the Supplemental Material [39]). The final result for the NMR splitting ν_Q can be expressed in the following form:

$$\nu_Q(\theta = 0) = \frac{eQ}{2h}S_{xxxx}\epsilon_b, \quad (2)$$

$$\frac{\nu_Q(\theta, \phi)}{\nu_Q(\theta = 0)} = \sum_{i=1}^{4} A_i(\theta, \phi), \quad (3)$$

$$A_1(\theta, \phi) = 1 - \frac{3}{2}\sin^2\theta, \quad (4)$$

$$A_2(\theta, \phi) = \frac{3}{4}\sin^2\theta\frac{\epsilon_\eta \cos 2\phi}{\epsilon_b}, \quad (5)$$

$$A_3(\theta, \phi) = 2\sin^2\theta\frac{\epsilon_{xy}\sin 2\phi}{\epsilon_b}\frac{S_{yzyz}}{S_{xxxx}}, \quad (6)$$

$$A_4(\theta, \phi) = 2\sin 2\theta\frac{\epsilon_{xz}\cos\phi + \epsilon_{yz}\sin\phi}{\epsilon_b}\frac{S_{yzyz}}{S_{xxxx}}. \quad (7)$$

The quadrupolar NMR shifts are insensitive to purely hydrostatic strain (with $\epsilon_{xx} = \epsilon_{yy} = \epsilon_{zz}$), so we can simplify the calculations by neglecting the hydrostatic part $\epsilon_h = \epsilon_{xx} + \epsilon_{yy} +$

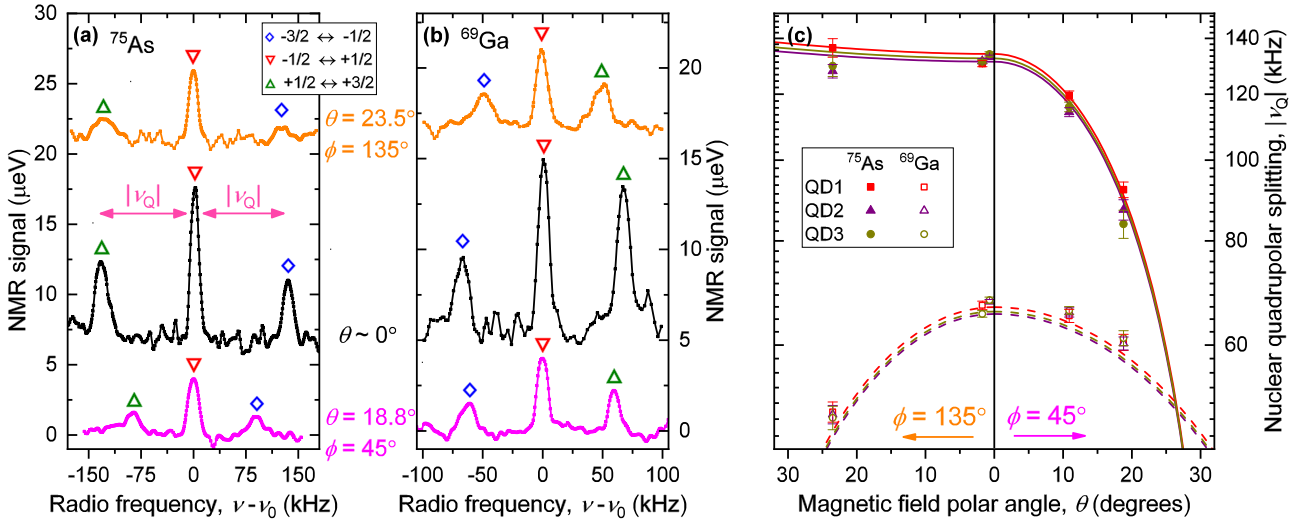

FIG. 2. (a), (b) Nuclear magnetic resonance spectra of ^{75}As (a) and ^{69}Ga (b) nuclei in an individual GaAs/AlGaAs quantum dot QD2 in a uniaxially stressed sample. The spectra were measured in large static magnetic field $B_0 \approx 8$ T corresponding to $\nu_0 \approx 58.55$ MHz for ^{75}As and $\nu_0 \approx 82.05$ MHz for ^{69}Ga. Three different directions of the field are used: aligned along the sample growth direction ($\theta \sim 0$, middle spectra), tilted by $\theta = 23.5°$ towards the $[1\bar{1}0]$ crystal axis ($\phi = 135°$, top traces), and tilted by $\theta = 18.8°$ towards the [110] crystal axis ($\phi = +45°$, bottom traces). Each line of the NMR triplet corresponds to a distinct magnetic dipolar transition $-3/2 \leftrightarrow -1/2$ ($\diamond$), $-1/2 \leftrightarrow +1/2$ ($\triangledown$), and $+1/2 \leftrightarrow +3/2$ ($\triangle$). The tilting of magnetic field ($\theta > 0$) is seen to modify the nuclear quadrupolar splitting ν_Q between the central peak $-1/2 \leftrightarrow +1/2$ and the satellite peaks $\pm 1/2 \leftrightarrow \pm 3/2$. (c) Experimentally measured magnitude of the quadrupolar splitting $|\nu_Q|$ of ^{75}As (solid symbols) and ^{69}Ga (open symbols) nuclei as a function of the polar angle θ for magnetic field tilted towards $[1\bar{1}0]$ ($\phi = 135°$, left part) or [110] ($\phi = 45°$, right part). Results are shown for three individual quantum dots: QD1 (squares), QD2 (triangles), and QD3 (circles). Error bars are 95% confidence intervals. Lines show the ν_Q dependence for ^{75}As (solid lines) and ^{69}Ga (dashed lines) calculated according to Eqs. (2)–(7) with best fitted parameters.

$\epsilon_{zz} = 0$ and the three diagonal strains are then completely defined by the biaxial strain $\epsilon_b = \epsilon_{zz} - (\epsilon_{xx} + \epsilon_{yy})/2$ and the deviatoric strain $\epsilon_\eta = \epsilon_{xx} - \epsilon_{yy}$.

Equations (2)–(7) are valid for any sufficiently small strain ϵ_{ij}. One particularly useful case is the strain induced by a uniaxial stress P in the xy plane making angle ξ with the x axis ($P < 0$ corresponds to compression). Using Hooke's law we find that such stress results in strain of the following form:

$$\epsilon_b^P = -P/(2c_{11} - 2c_{12}), \tag{8}$$

$$\epsilon_\eta^P/\epsilon_b^P = -2\cos 2\xi, \tag{9}$$

$$\epsilon_{xy}^P/\epsilon_b^P = -(c_{11} - c_{12})\sin 2\xi/(2c_{44}), \tag{10}$$

$$\epsilon_{xz}^P = \epsilon_{yz}^P = 0, \tag{11}$$

where $c_{11} = 118.8$ GPa, $c_{12} = 53.8$ GPa, and $c_{44} = 59.4$ GPa are the known stiffness constants of GaAs [40].

IV. EXPERIMENTAL RESULTS FOR STRESSED SAMPLE

We have studied three individual quantum dots (QD1–QD3) from the uniaxially stressed sample piece. NMR spectra of an individual dot QD2 are shown in Fig. 2 for ^{75}As (a) and ^{69}Ga (b) nuclei, and exhibit triplet structure arising from the stress-induced quadrupolar effects [36–38]. Gaussian line shape fitting is used to determine the resonance frequencies and the quadrupolar splitting ν_Q of the $\pm 1/2 \leftrightarrow \pm 3/2$ satellite transitions from the $-1/2 \leftrightarrow +1/2$ central transition. For magnetic field along the [001] crystallographic direction ($\theta \approx 0$, middle spectra) we find $|\nu_Q| \approx 133.0$ kHz (≈ 67.7 kHz) for ^{75}As (^{69}Ga). In the case of ^{75}As tilting of the static field towards the direction of stress ([110], $\phi = +45°$) results in a pronounced reduction of ν_Q [Fig. 2(a), bottom spectrum]. By contrast tilting the field towards $[1\bar{1}0]$ ($\phi = 135°$) leaves ν_Q almost unchanged [Fig. 2(a), top spectrum]. The effect is different for ^{69}Ga, where the reduction in quadrupolar splitting ν_Q is very similar for $\phi = +45°$ and $\phi = 135°$ as observed in Fig. 2(b). The results are consistent for all three individual quantum dots and are summarized in Fig. 2(c), where experimentally measured $|\nu_Q|$ are shown by the symbols as a function of magnetic field direction polar angle θ for $\phi = +45°$ (right half of the graph) and for $\phi = 135°$ (left half).

Prior to presenting full numerical evaluation we use Eqs. (2)–(7) to analyze qualitatively the results of Fig. 2. The quadrupolar splitting at $\theta = 0$ [Eq. (2)] is governed only by the S_{xxxx} component of the gradient-elastic tensor and the biaxial strain ϵ_b, but is independent of other strain tensor components. These properties of $\nu_Q(\theta = 0)$ have been used in our previous work [8] for accurate derivation of S_{xxxx}. The quadrupolar splitting $\nu_Q(\theta, \phi)$ at finite tilt θ is proportional to $\nu_Q(\theta = 0)$ according to Eq. (3). The effect of oblique magnetic field is described by the angular factor, which is a sum of the four terms $A_i(\theta, \phi)$ ($i = 1 \ldots 4$) with different angular dependence. According to Eq. (4), $A_1(\theta, \phi) \leqslant 1$ and does not depend on the angle ϕ or S_{ijkl}, so this term always decreases ν_Q at a finite tilt θ. According to Eq. (9), $\epsilon_\eta = 0$ for the uniaxial stress along [110] ($\xi = +45°$) used in this work; moreover,

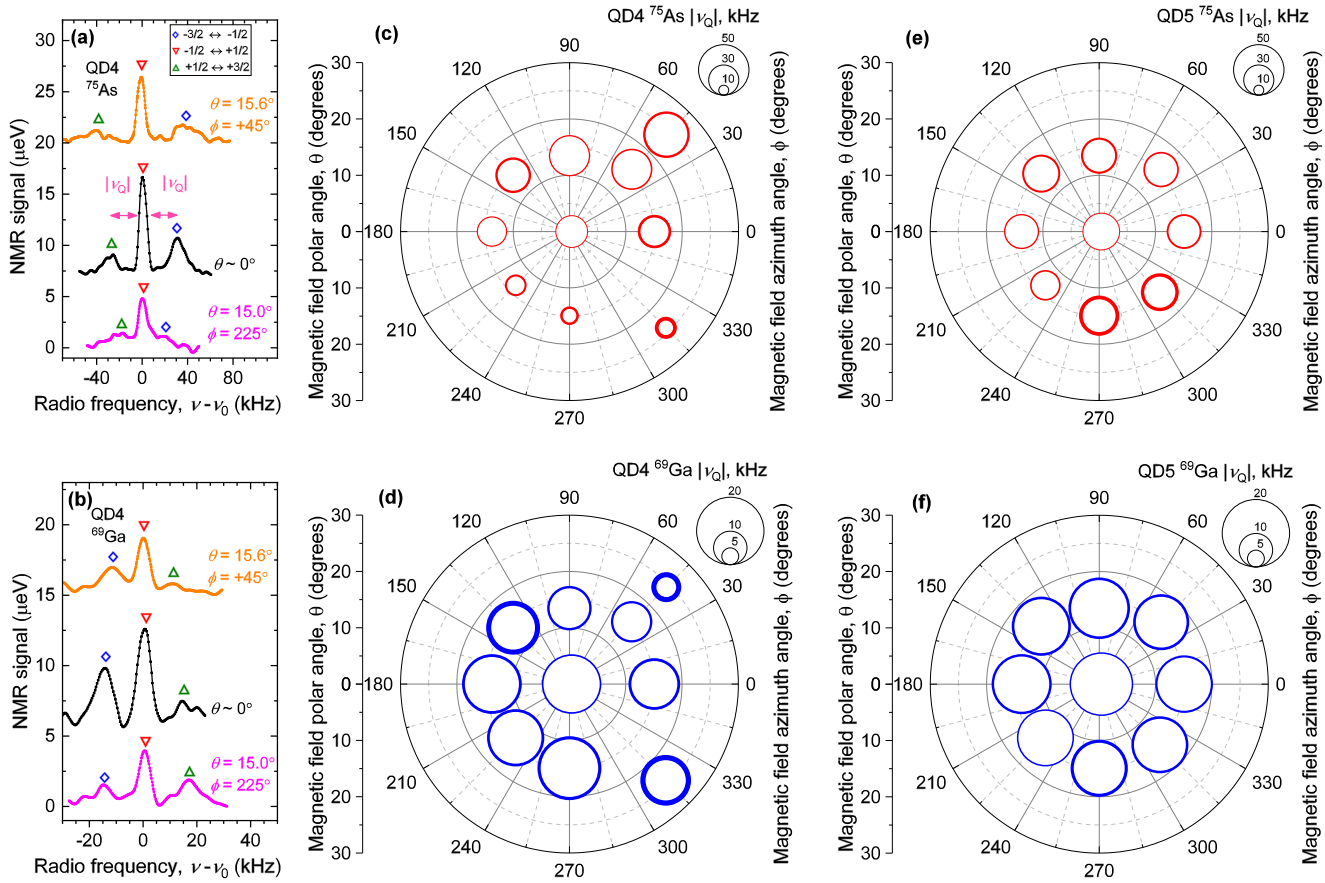

FIG. 3. (a), (b) Nuclear magnetic resonance spectra of ^{75}As (a) and ^{69}Ga (b) nuclei in an individual GaAs/AlGaAs quantum dot QD4 measured in an unstressed sample at $B_0 \approx 8$ T and different orientation angles θ, ϕ of the static magnetic field. The tilting of magnetic field ($\theta > 0$) is seen to modify the nuclear quadrupolar splitting ν_Q between the central peak $-1/2 \leftrightarrow +1/2$ and the satellite peaks $\pm 1/2 \leftrightarrow \pm 3/2$. (c), (d) Bubble plots of the quadrupolar splitting $|\nu_Q|$ measured on QD4 for ^{75}As (c) and ^{69}Ga (d) nuclei as a function of the polar angle θ and azimuth angle ϕ defining the direction of the static magnetic field with respect to sample crystallographic axes. The inner (outer) diameter of each bubble gives the lower (upper) bound of the 95% confidence interval for $|\nu_Q|$. (e), (f) Same as (c) and (d) but for another individual dot QD5.

$\partial\epsilon_\eta/\partial\xi = 0$ at $\xi = +45^\circ$ so the term $A_2(\theta, \phi)$ vanishes and is insensitive to small systematic errors in ξ. The term $A_4(\theta, \phi)$ also vanishes at $\xi = +45^\circ$ according to Eq. (9). According to Eqs. (6) and (10) the remaining term $A_3(\theta, \phi)$ has zero derivatives with respect to ξ and ϕ at $\xi = 45^\circ$ and $\phi = 45^\circ$ or $\phi = 135^\circ$, again making it insensitive to small angular errors. This choice of ξ and ϕ also maximizes the dependence of $A_3(\theta, \phi)$ on S_{yzyz} resulting in $A_3(\theta, \phi) = \mp \frac{c_{11}-c_{12}}{c_{44}} \frac{S_{yzyz}}{S_{xxxx}} \sin^2\theta$ at $\phi = 45^\circ$ ($\phi = 135^\circ$) and making this experimental configuration best suited for derivation of S_{yzyz}/S_{xxxx}.

In Fig. 2(c) $|\nu_Q|$ of ^{75}As is almost unaffected by θ at $\phi = 135^\circ$, signifying that the decrease in A_1 is compensated by an increase in A_3 and hence $S_{yzyz}/S_{xxxx} > 0$ for ^{75}As. For $\phi = 45^\circ$ both A_1 and A_3 decrease explaining the pronounced reduction in ^{75}As $|\nu_Q|$ with increasing tilt angle θ. By contrast, the reduction of ^{69}Ga $|\nu_Q|$ is somewhat stronger at $\phi = 135^\circ$, revealing that $S_{yzyz}/S_{xxxx} < 0$ for ^{69}Ga. On the other hand, the difference between $\phi = 45^\circ$ and $\phi = 135^\circ$ is small for ^{69}Ga, suggesting that $|S_{yzyz}/S_{xxxx}|$ of ^{69}Ga is significantly smaller than in the case of ^{75}As. In what follows we confirm and quantify these conclusions.

V. EXPERIMENTAL RESULTS FOR UNSTRESSED SAMPLE

We have studied two individual quantum dots (QD4, QD5) from the as-grown (unstressed) sample piece. NMR spectra of an individual dot QD4 are shown in Fig. 3 for ^{75}As (a) and ^{69}Ga (b) nuclei, and exhibit triplet structure arising from quadrupolar effects induced by the built-in (intrinsic) strain. Gaussian line shape fitting is used to determine the resonance frequencies and the quadrupolar splitting ν_Q of the $\pm 1/2 \leftrightarrow \pm 3/2$ satellite transitions from the $-1/2 \leftrightarrow +1/2$ central transition. As in the case of the uniaxially stressed sample, the quadrupolar splitting ν_Q depends on the orientation of the static magnetic field (described by the angles θ and ϕ). However, both the ν_Q and the changes with θ and ϕ are considerably smaller than in the stressed sample due to the smallness of the built-in strain in the nearly lattice matched GaAs/AlGaAs heterostructures.

In order to probe the built-in strain of the quantum dots we have systematically measured the dependence of NMR splitting ν_Q on θ and ϕ for ^{75}As and ^{69}Ga nuclei in QD4. The results are shown in Figs. 3(c) and 3(d), respectively,

as bubble plots in polar coordinates, where each bubble is centered at the corresponding $(\theta,\ \phi)$ point, while its diameter is proportional to $|\nu_Q|$. The plots reveal certain systematic trends. For example, $|\nu_Q|$ of ^{75}As increases when the field is tilted along the $\phi = 45^\circ$ or $\phi = 90^\circ$ direction, but decreases for the opposite ($\phi \to \phi + 180^\circ$) direction $\phi = 225^\circ$ or $\phi = 270^\circ$ [Fig. 3(c)]. From Eqs. (4)–(7), we find that $A_4(\theta, \phi)$ is the only term permitting different responses to magnetic field projection directed along ϕ and $\phi + 180^\circ$. Therefore, at least one of the strain components ϵ_{xz} and ϵ_{yz} is not zero in QD4, which, as we show below quantitatively, signifies that the principal direction of strain is not aligned with the growth axis. For ^{69}Ga [Fig. 3(c)] the asymmetry is reversed, with $|\nu_Q|$ increasing (decreasing) for $\phi = 225^\circ$ and $\phi = 270^\circ$ ($\phi = 45^\circ$ and $\phi = 90^\circ$), confirming that the signs of S_{yzyz}/S_{xxxx} are opposite for As and Ga. Similar detailed NMR measurements are shown for another dot QD5 in Figs. 3(e) and 3(f), where a more symmetric picture is observed revealing that each quantum dot has its individual strain profile.

VI. QUANTITATIVE ANALYSIS

According to Eqs. (2)–(7) the response of the nuclear quadrupolar splitting ν_Q to the orientation of the static magnetic field $(\theta,\ \phi)$ encodes information on the strain field within the quantum dot volume and the material parameters $S_{yzyz},\ S_{xxxx}$. We now show how both can be determined from the NMR experiments. To this end we use Eqs. (2)–(7) to model simultaneously the ν_Q values measured on the unstressed and stressed samples. We take the known values of $c_{11},\ c_{12},\ c_{44}$ [40], and S_{xxxx} [8]. The model (fitting) parameters include the ratios of S_{yzyz}/S_{xxxx} for ^{75}As and ^{69}Ga, and the five components $\epsilon_b,\ \epsilon_\eta,\ \epsilon_{xy}, \epsilon_{xz},\ \epsilon_{yz}$ of the built-in (intrinsic) strain ϵ^{int} for each unstressed quantum dot (QD4 and QD5). Since the stiffness constants c_{11}, c_{12}, and c_{44} of GaAs and AlGaAs are very similar [40], we have with good accuracy that the total strain in the stressed dots is a sum of the intrinsic strain ϵ^{int} and the extrinsic strain ϵ^{ext} induced by the stress:

$$\epsilon^{\text{tot}} = \epsilon^{\text{int}} + \epsilon^{\text{ext}}. \tag{12}$$

The stressed sample is $\sim$1 mm in dimensions, while quantum dots are only $\sim$100 nm from the top surface. Thus according to the Saint-Venant's principle the dots are effectively at a traction-free (unloaded) surface. This surface is a (001) crystallographic plane (xy plane) and the free-surface boundary conditions ensure the absence of the out-of-plane (z-directed) forces. Moreover, the studied quantum dots are close ($\sim$10 μm) to the edge of the sample marked by the dash-dotted line in Fig. 1. Thus, in a similar manner, the forces out of the $(1\bar{1}0)$ plane are zero or small; hence the extrinsic stress acting on the dots is close to uniaxial with [110] ($\xi = 45^\circ$) as a principal axis. This is further verified by observing that GaAs substrate PL [8] is linearly polarized along the $\xi \approx 46.5^\circ$ direction, which gives an estimate of the actual major stress direction. For these reasons for each of the stressed dots QD1–QD3, we can accurately model ϵ^{ext} using Eqs. (8)–(11) for the strain ϵ^P under purely uniaxial stress with stress magnitudes P used as fitting parameters. Finally, in our experiments it is not possible to measure the same quantum dot with and without stress; therefore, ϵ^{int} in the stressed quantum dots is unaccessible and some additional assumption is needed. We assume that ϵ_b^{int} in the stressed dots equals the average of ϵ_b^{int} in the unstressed dots QD4, QD5. By contrast, the remaining components of intrinsic strain in the stressed dots are neglected ($\epsilon_\eta^{\text{int}} = \epsilon_{xy}^{\text{int}} = \epsilon_{xz}^{\text{int}} = \epsilon_{yz}^{\text{int}} = 0$)—the validity of this assumption is justified in what follows based on the fitting results.

The least square best fit is found by minimizing the weighted sum χ^2 of the squared differences between the measured quadrupolar splittings ν_Q [Figs. 2(c) and 3(c)–3(f)] and the ν_Q predicted by the model [Eqs. (2)–(7)]. We find good agreement between the model and the data, with the root mean square fit residual of $\approx$1.9 kHz, comparable to the accuracy in the experimentally measured ν_Q values. The best fit model for the dots in the stressed sample is shown by the lines in Figs. 2(c) in good agreement with experiment. In order to estimate the errors in the fitted parameters we use the Monte Carlo approach, where the χ^2 sum is calculated for a large number of random sets of the fitting parameters. Moreover, we account for any possible systematic errors by randomly varying in a small range the direction of the static field ($\pm 1^\circ$ for the ϕ values and $\pm 0.5^\circ$ for θ) and the stress ($\pm 1^\circ$ for ξ). We then form the estimates of the confidence regions by selecting the parameter combinations with $\chi^2 < \chi^2_{\text{min}} + Q_\gamma$, where χ^2_{min} is the best fit χ^2 value and Q_γ is the quantile of the χ^2 distribution corresponding to the confidence level $1 - \gamma = 95\%$ (Chap. 9 in Ref. [41]). The confidence interval of an individual parameter is then derived as maximum and minimum values of this parameter within the overall multidimensional confidence region.

The best fit for the stress magnitude exerted by the stress mount is $P \approx -140$ MPa for the three studied dots QD1–QD3. The 95% confidence estimates for the ratios of the gradient elastic tensor components are $\frac{S_{yzyz}}{S_{xxxx}} = 1.98^{+0.21}_{-0.27}$ for ^{75}As and $\frac{S_{yzyz}}{S_{xxxx}} = -0.40^{+0.23}_{-0.31}$ for ^{69}Ga. Using these ratios and our previous measurements [8] of $QS_{xxxx} \approx +0.758 \times 10^{-6}$ V for ^{75}As and $QS_{xxxx} \approx -0.377 \times 10^{-6}$ V for ^{69}Ga, we estimate the off-diagonal components of the gradient-elastic tensor (multiplied by the corresponding quadrupolar moment Q) of GaAs as $QS_{yzyz} \approx +1.51 \times 10^{-6}$ V for ^{75}As and $QS_{yzyz} \approx +0.151 \times 10^{-6}$ V for ^{69}Ga.

The components of the intrinsic strain ϵ^{int} in the unstressed dots are also obtained from the fit. In order to derive their physical meaning we recall that strain tensor is symmetric and hence can be diagonalized to find the three principal strains (eigenvalues) ϵ_1, ϵ_2, ϵ_3 and their directions (eigenvectors). We choose as ϵ_3 the component whose direction is closest to the sample growth axis z. Since the eigenvectors are mutually orthogonal and hydrostatic strain can be neglected ($\epsilon_1 + \epsilon_2 + \epsilon_3 = 0$), the remaining principal strains can be fully characterized by the difference $|\epsilon_1 - \epsilon_2|$ and the direction of the eigenvector corresponding to the larger of ϵ_1 and ϵ_2. The fitted ϵ_3 magnitudes are found to be $(2.41^{+0.25}_{-0.29}) \times 10^{-4}$ for QD4 and $(2.65^{+0.14}_{-0.14}) \times 10^{-4}$ for QD5. The directions of the ϵ_3 component are shown in Fig. 4(a) for QD4 and Fig. 4(c) for QD5, where best fit values are shown by the stars and the samplings of the 95% confidence regions are shown by the dots. The magnitudes of $|\epsilon_1 - \epsilon_2|$ and the direction of the larger of ϵ_1 and ϵ_2 are shown in Fig. 4(b) for QD4 and Fig. 4(d) for QD5.

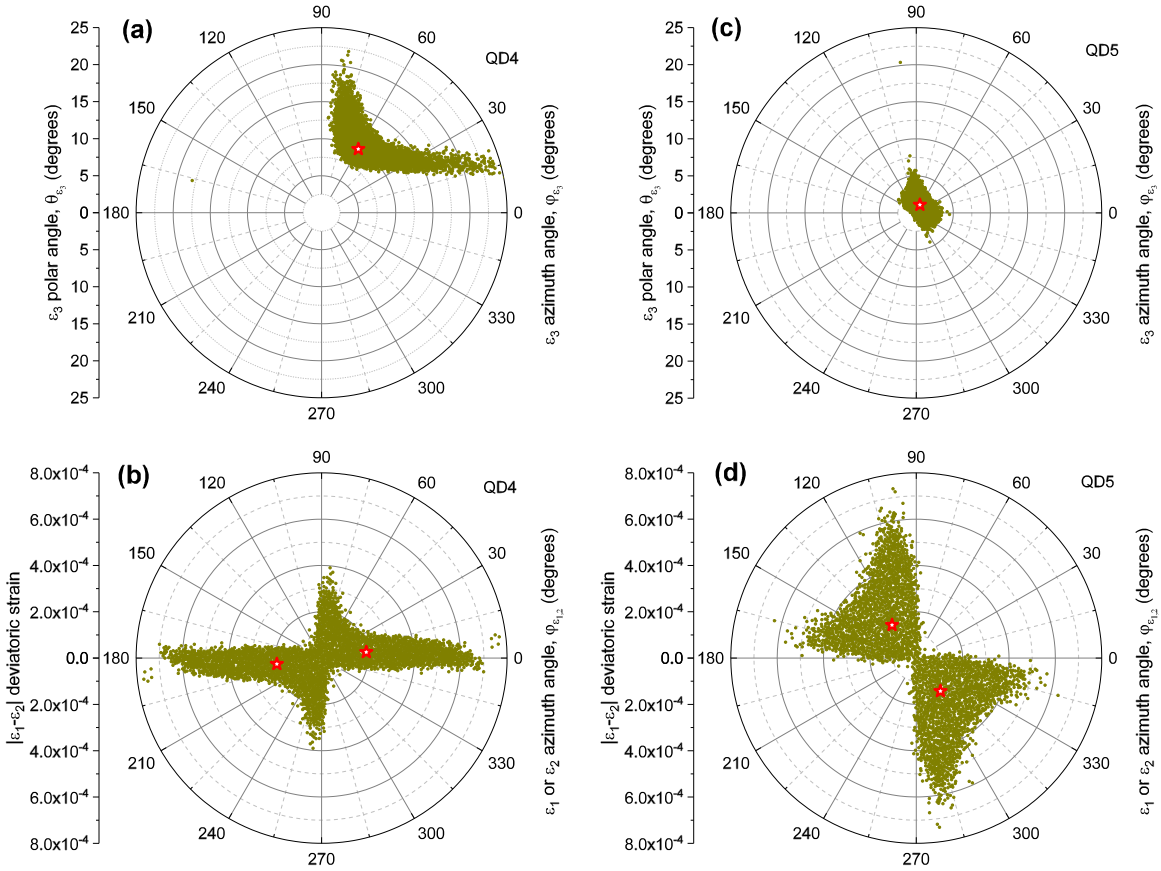

FIG. 4. Reconstruction of the strain tensor parameters in GaAs/AlGaAs quantum dots in the as-grown (unstressed) sample. Stars show best fit estimates and points show Monte Carlo sampling of the 95% confidence region. The strain tensors ϵ^{int} derived from fitting of the NMR splittings ν_Q are diagonalized to find the magnitudes of the principal strain components ϵ_1, ϵ_2, ϵ_3 and their orientation angles θ_{ϵ_i}, ϕ_{ϵ_i} with respect to crystallographic coordinate system xyz. (a) Polar plot of the direction of the strain principle component ϵ_3 in QD4. (b) Polar plot showing the difference $|\epsilon_1 - \epsilon_2|$ (radial axis) as a function of the azimuth angle $\phi_{\epsilon_{1,2}}$ of the largest of the principal strains ϵ_1 and ϵ_2 (angular axis) for QD4. Since eigenvectors are defined up to a constant factor, each point on the plot at angle $\phi_{\epsilon_{1,2}}$ is accompanied by another point at $\phi_{\epsilon_{1,2}} + 180^\circ$. (c), (d) Same as (a) and (b) but for another individual dot QD5.

The results of Figs. 4(a) and 4(c) show that the orientation of the ϵ_3 principal strain axis can be deduced with good accuracy. In QD5 the ϵ_3 direction is very close to the [001] axis [$\theta_{\epsilon_3} \approx 1^\circ$, Fig. 4(c)], which is expected since the growth direction is a symmetry axis of the planar GaAs/AlGaAs structure. By contrast, QD4 shows a small [$\theta_{\epsilon_3} \approx 10^\circ$, Fig. 4(a)] but reliably detectable tilting of the principal axis, in agreement with the qualitative observation of the asymmetric changes in ν_Q in Figs. 3(c) and 3(d). Quantum dots QD4 and QD5 are only $\sim$10 μm apart, so their difference is most likely due to the localized variations in growth conditions: for example, an imperfect shape of the etched nanohole that led to formation of QD4. The magnitudes of ϵ_3 are also derived with good accuracy and are very similar for QD4 and QD5. The situation is very different for the ϵ_1 and ϵ_2 parameter estimates: Figs. 4(b) and 4(d) show a large spread in the $|\epsilon_1 - \epsilon_2|$ confidence region ranging from $\approx$0, corresponding to an axially symmetric (biaxial) strain, to $\approx 6 \times 10^{-4}$, which is a factor of 3 larger than the ϵ_3 magnitude. Moreover, the predominant orientations of the ϵ_1 and ϵ_2 strains are different for QD4 ($\phi_{\epsilon_{1,2}} \approx 0^\circ$, $\phi_{\epsilon_{1,2}} \approx 180^\circ$) and QD5 ($\phi_{\epsilon_{1,2}} \approx 135^\circ$, $\phi_{\epsilon_{1,2}} \approx 315^\circ$). This is in stark contrast to the similarity of the ϵ_3 parameters between these two dots. Our interpretation is that $|\epsilon_1 - \epsilon_2| \approx 0$ in both dots, which is within the confidence intervals, and agrees with the most likely scenario that the strain is induced by the residual mismatch of the GaAs and AlGaAs layers, which has no preferential direction in the xy coordinate plane. The reason for the reduced accuracy in ϵ_1 and ϵ_2 estimates is that these strain components are controlled by the terms A_1 ... A_3 [Eqs. (4)–(6)], which scale as $\propto\theta^2$ at $\theta \to 0$. By contrast the A_4 term [Eq. (7)], which determines the ϵ_3 tilt through the ϵ_{xz} and ϵ_{yz} components, scales as $\propto\theta$. As a result the quadrupolar NMR splitting ν_Q is dominated by A_4 in the range of angles $\theta \lesssim 25^\circ$ used in our experiments.

VII. DISCUSSION AND CONCLUSIONS

We have demonstrated experimental reconstruction of the strain field in individual GaAs/AlGaAs quantum dots using NMR spectroscopy at different magnetic field orientations. This approach permits strain profiling of a nanoscale semiconductor quantum dot without any preliminary assumptions about the internal structure and in a nondestructive manner, i.e., unlike in electron and atomic force microscopies both the optical and structural properties can be examined for the same quantum dot. Currently, the method has a higher accuracy

for the components of strain parallel to the structure growth and lower accuracy for the in-plane strain. This is due to the relatively small range of the available orientations of magnetic field ($\theta \lesssim 25^\circ$), imposed by the need for high nuclear spin polarization degree, which is only achievable via optical pumping close to Faraday configuration [32] ($\theta = 0$), where strict spin selection rules exist for the electron-hole optical transitions. However, this is not a fundamental limitation: owing to the long nuclear spin lifetimes [42,43] in GaAs/AlGaAs semiconductor nanostructures, it is possible in principle to polarize the nuclear spins in Faraday geometry first and then tilt the sample mechanically to an arbitrary target angle θ for rf excitation (Fig. 5). Such periodic switching between two geometries can be achieved in an apparatus where the micro-PL objective and the NMR rf coil are static, while the sample can rotate between two stable positions controlled for example by sending dc current through an additional coil attached to the sample mount and interacting with the strong static field B_0. By adding NMR measurements at $\theta \approx 90^\circ$ it would be possible to achieve high accuracy for all components of strain. We also point out that the estimates derived here are for the average strain—the strain field varies within the quantum dot volume, observed as finite broadening of the $\pm 3/2 \leftrightarrow \pm 1/2$ satellite NMR peaks. Analysis of the satellite peak broadening at different magnetic field directions might be used for reconstruction of the inhomogeneous strain distribution within the nanoscale volume. Similar NMR strain profiling approach can be envisaged for self-assembled quantum dots, although this would likely require model assumptions [21,22] and/or additional structural information (e.g., transmission electron microscopy) [19] due to the large inhomogeneity of strain.

By extending NMR spectroscopy in oblique fields to the uniaxially stressed quantum dots we are able to derive the S_{yzyz} components of the GaAs gradient elastic tensors. NMR spectra are measured here in three geometries: (i) $\theta \approx 0$; (ii) $\theta > 0$, $\xi \approx +45^\circ$, $\phi \approx 135^\circ$; (iii) $\theta > 0$, $\xi \approx +45^\circ$, $\phi \approx +45^\circ$. While configuration (i) combined with either (ii) or (iii) is sufficient to determine S_{yzyz}, we use all three geometries in order to verify the validity of the theoretical model and improve the accuracy. We note that, according to Eqs. (2)–(7), it is the ratios S_{yzyz}/S_{xxxx} that are measured from the angular dependence of the quadrupolar splitting ν_Q—these ratios could be derived accurately in our experiments even if the absolute values of strain and/or S_{xxxx} were not known. Lower accuracy of the estimates for intrinsic principal strains ϵ_1 and ϵ_2 is the reason we neglect all strain components except for $\epsilon_b^{\rm int}$ when modeling strain in the stressed dots [Eq. (12)]. However, we have verified that taking into account all $\epsilon^{\rm int}$ components has little effect on the fitted S_{yzyz}/S_{xxxx} values—the same low sensitivity of ν_Q to $\epsilon_{xy}^{\rm int}$ and $\epsilon_\eta^{\rm int}$ that reduces the accuracy of ϵ_1 and ϵ_2 estimates means that S_{yzyz}/S_{xxxx} estimates are largely unaffected by this inaccuracy. We further point out that we avoid Voigt notations in this work: while $S_{11} = S_{xxxx}$ unambiguously, the conversion from S_{yzyz} to S_{44} requires an additional factor of 2 in the definition of the nondiagonal strain components, which might be a source of confusion. For that reason all S_{ijkl} and ϵ_{ij} quantities reported here are proper tensors, i.e., they transform as tensors under affine coordinate transformations.

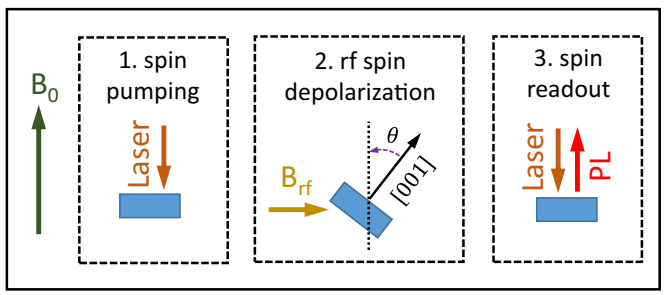

FIG. 5. Proposed scheme for optically detected NMR measurements at arbitrary sample tilt angles θ. The experimental cycle consists of (1) optical nuclear spin pumping in Faraday geometry (no sample tilt), (2) tilting the sample to the desired angle θ and applying the rf pulse depolarizing the nuclear spins, and (3) returning the sample to Faraday geometry to perform optical readout of the nuclear spin polarization. Separation of stages (1) and (2) is possible due to the long nuclear spin lifetimes, and removes the restrictions arising from suppressed optical nuclear spin pumping at large θ.

Our NMR based estimate $S_{yzyz}/S_{xxxx} \approx +1.98$ for ^{75}As matches $S_{44}/S_{11} \approx +2.0$ measured previously via NAR [4], whereas our $S_{yzyz}/S_{xxxx} \approx -0.40$ for ^{69}Ga is considerably different from $S_{44}/S_{11} \approx -1.0$ of Ref. [4]. Given that our NMR values of S_{xxxx} are a factor of $\approx$1.4 smaller [8] than those derived in NAR, there is a considerable disagreement, as large as a factor of $\approx$3.5 for QS_{yzyz} of gallium. Sundfors [4] conducted NAR experiments at 300 K, whereas our measurements were performed at a low temperature of 4.2 K. However, temperature is unlikely to cause such discrepancy, since even in hexagonal metals [44,45] the change in EFGs between 0 and 300 K is only 10% –20%. Besides, for InSb there is a good agreement between the room temperature [4] and low temperature [6] (77 K) measurements. The differences in sample background doping are also unlikely to play any role, since lattice deformations induced by carriers are small ($\lesssim 10^{-5}$) even in quantum dots [46] where electrons and holes are strongly localized—this is supported by the agreement in QS_{ijkl} found in two experimental studies [4,6] on bulk InSb samples with carrier concentration differing by a factor of $\sim$70. While there is an agreement for InSb, the QS_{ijkl} values of other semiconductors (GaSb, InAs, AlSb) obtained from NAR [4] are systematically larger than those found from static-strain bulk sample NMR [6,7], just as they are larger than our static-strain NMR values obtained on GaAs QDs. It is worth noting that InSb has large gradient-elastic tensor components S_{ijkl} and both In and Sb atoms have large quadrupolar moments Q. The absorption of acoustic waves by the nuclear spins scales as [4] $\propto Q^2 S_{ijkl}^2$, making NAR experiments more reliable for InSb. Any additional absorption mechanisms, unrelated to nuclear spins, would lead to overestimated S_{ijkl}, especially for nuclei with small Q (such as gallium). Thus it is likely that the gradient-elastic tensors S_{ijkl} derived for GaAs from NAR [4] were overestimated due to such parasitic absorption. The NMR measurements employed here are based on direct detection of the nuclear quadrupolar spectral shifts, making them immune to such systematic errors. Moreover, our MBE-grown semiconductor structures benefit from high crystal quality, not achievable at the time of the previous studies. The revised complete gradient-elastic tensors of GaAs reported here can be used for more accurate description of the strain-related nuclear spin effects.

ACKNOWLEDGMENTS

The authors are grateful to Y. Huo, S. F. Covre da Silva, X. Yuan, and C. McEwan for their assistance. This work was supported by the EPSRC Programme Grant No. EP/N031776/1, the Linz Institute of Technology (LIT), and the Austrian Science Fund (FWF): Grant No. P 29603. E.A.C. was supported by the Royal Society via a University Research Fellowship.

[1] R. J. Harrison and P. L. Sagalyn, Phys. Rev. **128**, 1630 (1962).

[2] C. Brusewitz, U. Vetter, and H. Hofsass, J. Phys.: Condens. Matter **27**, 055401 (2015).

[3] R. K. Sundfors, Phys. Rev. **177**, 1221 (1969).

[4] R. K. Sundfors, Phys. Rev. B **10**, 4244 (1974).

[5] R. K. Sundfors and R. K. Tsui, Phys. Rev. B **12**, 790 (1975).

[6] V. L. Bogdanov and V. V. Lemanov, Fiz. Tverd. Tela. **9**, 469 (1967) [Sov. Phys. Solid State **9**, 357 (1967)].

[7] V. L. Bogdanov and V. V. Lemanov, Fiz. Tverd. Tela. **10**, 212 (1968) [Sov. Phys. Solid State **10**, 159 (1968)].

[8] E. A. Chekhovich, I. M. Griffiths, M. S. Skolnick, H. Huang, S. F. Covre da Silva, X. Yuan, and A. Rastelli, Phys. Rev. B **97**, 235311 (2018).

[9] C.-W. Huang and X. Hu, Phys. Rev. B **81**, 205304 (2010).

[10] E. A. Chekhovich, M. Hopkinson, M. S. Skolnick, and A. I. Tartakovskii, Nat. Commun. **6**, 6348 (2015).

[11] A. Bechtold, D. Rauch, F. Li, T. Simmet, P.-L. Ardelt, A. Regler, K. Müller, N. A. Sinitsyn, and J. J. Finley, Nat. Phys. **11**, 1005 (2015).

[12] G. Wüst, M. Munsch, F. Maier, A. V. Kuhlmann, A. Ludwig, A. D. Wieck, D. Loss, M. Poggio, and R. J. Warburton, Nat. Nanotechnol. **11**, 885 (2016).

[13] T. Botzem, R. P. G. McNeil, J.-M. Mol, D. Schuh, D. Bougeard, and H. Bluhm, Nat. Commun. **7**, 11170 (2016).

[14] R. Stockill, C. Le Gall, C. Matthiesen, L. Huthmacher, E. Clarke, M. Hugues, and M. Atature, Nat. Commun. **7**, 12745 (2016).

[15] D. Gangloff, G. Éthier-Majcher, C. Lang, E. Denning, J. Bodey, D. Jackson, E. Clarke, M. Hugues, C. Le Gall, and M. Atature, arXiv:1812.07540.

[16] E. A. Chekhovich, K. V. Kavokin, J. Puebla, A. B. Krysa, M. Hopkinson, A. D. Andreev, A. M. Sanchez, R. Beanland, M. S. Skolnick, and A. I. Tartakovskii, Nat. Nanotechnol. **7**, 646 (2012).

[17] M. Munsch, G. Wust, A. V. Kuhlmann, F. Xue, A. Ludwig, D. Reuter, A. D. Wieck, M. Poggio, and R. J. Warburton, Nat. Nanotechnol. **9**, 671 (2014).

[18] K. Flisinski, I. Y. Gerlovin, I. V. Ignatiev, M. Y. Petrov, S. Y. Verbin, D. R. Yakovlev, D. Reuter, A. D. Wieck, and M. Bayer, Phys. Rev. B **82**, 081308 (2010).

[19] P. S. Sokolov, M. Y. Petrov, T. Mehrtens, K. Müller-Caspary, A. Rosenauer, D. Reuter, and A. D. Wieck, Phys. Rev. B **93**, 045301 (2016).

[20] M. S. Kuznetsova, K. Flisinski, I. Y. Gerlovin, M. Y. Petrov, I. V. Ignatiev, S. Y. Verbin, D. R. Yakovlev, D. Reuter, A. D. Wieck, and M. Bayer, Phys. Rev. B **89**, 125304 (2014).

[21] C. Bulutay, Phys. Rev. B **85**, 115313 (2012).

[22] C. Bulutay, E. A. Chekhovich, and A. I. Tartakovskii, Phys. Rev. B **90**, 205425 (2014).

[23] R. M. Wood, J. T. Tokarski, L. A. McCarthy, C. J. Stanton, and C. R. Bowers, J. Appl. Phys. **120**, 085104 (2016).

[24] R. M. Wood, D. Saha, L. A. McCarthy, J. T. Tokarski, G. D. Sanders, P. L. Kuhns, S. A. McGill, A. P. Reyes, J. L. Reno, C. J. Stanton, and C. R. Bowers, Phys. Rev. B **90**, 155317 (2014).

[25] M. Eickhoff, B. Lenzmann, D. Suter, S. E. Hayes, and A. D. Wieck, Phys. Rev. B **67**, 085308 (2003).

[26] G. P. Flinn, R. T. Harley, M. J. Snelling, A. C. Tropper, and T. M. Kerr, Semicond. Sci. Technol. **5**, 533 (1990).

[27] J. Zhang, Y. Huo, A. Rastelli, M. Zopf, B. Höfer, Y. Chen, F. Ding, and O. G. Schmidt, Nano Lett. **15**, 422 (2015).

[28] M. Gong, W. Zhang, G.-C. Guo, and L. He, Phys. Rev. Lett. **106**, 227401 (2011).

[29] D. Huber, M. Reindl, S. F. Covre da Silva, C. Schimpf, J. Martín-Sánchez, H. Huang, G. Piredda, J. Edlinger, A. Rastelli, and R. Trotta, Phys. Rev. Lett. **121**, 033902 (2018).

[30] C. Heyn, A. Stemmann, T. Koppen, C. Strelow, T. Kipp, M. Grave, S. Mendach, and W. Hansen, Appl. Phys. Lett. **94**, 183113 (2009).

[31] P. Atkinson, E. Zallo, and O. G. Schmidt, J. Appl. Phys. **112**, 054303 (2012).

[32] E. A. Chekhovich, A. Ulhaq, E. Zallo, F. Ding, O. G. Schmidt, and M. S. Skolnick, Nat. Mater. **16**, 982 (2017).

[33] B. Urbaszek, X. Marie, T. Amand, O. Krebs, P. Voisin, P. Maletinsky, A. Högele, and A. Imamoglu, Rev. Mod. Phys. **85**, 79 (2013).

[34] E. A. Chekhovich, M. N. Makhonin, A. I. Tartakovskii, A. Yacoby, H. Bluhm, K. C. Nowack, and L. M. K. Vandersypen, Nat. Mater. **12**, 494 (2013).

[35] C. P. Slichter, *Principles of Magnetic Resonance* (Springer, Berlin, 1990).

[36] R. V. Pound, Phys. Rev. **79**, 685 (1950).

[37] J. L. Marsh and P. A. Casabella, Phys. Rev. **150**, 546 (1966).

[38] R. G. Shulman, B. J. Wyluda, and P. W. Anderson, Phys. Rev. **107**, 953 (1957).

[39] See Supplemental Material at http://link.aps.org/supplemental/10.1103/PhysRevB.99.125304 for derivation of the theoretical model equations .

[40] S. Adachi, *Properties of Semiconductor Alloys: Group-IV, III-V and II-VI Semiconductors* (Wiley, New York, 2009).

[41] G. Cowan, *Statistical Data Analysis* (Clarendon Press, London, 1998).

[42] A. Ulhaq, Q. Duan, E. Zallo, F. Ding, O. G. Schmidt, A. I. Tartakovskii, M. S. Skolnick, and E. A. Chekhovich, Phys. Rev. B **93**, 165306 (2016).

[43] A. E. Nikolaenko, E. A. Chekhovich, M. N. Makhonin, I. W. Drouzas, A. B. Van'kov, J. Skiba-Szymanska, M. S. Skolnick,

P. Senellart, D. Martrou, A. Lemaître, and A. I. Tartakovskii, Phys. Rev. B **79**, 081303 (2009).
[44] R. Raghavan and P. Raghavan, Phys. Lett. A **36**, 313 (1971).
[45] D. Torumba, K. Parlinski, M. Rots, and S. Cottenier, Phys. Rev. B **74**, 144304 (2006).
[46] S. Tiemeyer, M. Bombeck, H. Göhring, M. Paulus, C. Sternemann, J. Nase, F. J. Wirkert, J. Möller, T. Büning, O. H. Seeck, D. Reuter, A. D. Wieck, M. Bayer, and M. Tolan, Nanotechnology **27**, 425702 (2016).